Electronic Supplementary Information

Tetragonal $CoMn_2O_4$ nanocrystals on electrospun carbon fibers as a high–performance battery–type supercapacitor electrode material

Daniel M. Mijailović, [a] Vuk V. Radmilović, [b] Uroš Č. Lačnjevac, [c] Dušica B. Stojanović, [b] Karen C. Bustillo, [d] Vladimir D. Jović, [c] Velimir R. Radmilović, [b,e] and Petar S. Uskoković *[b]

[a] Innovation Center, Faculty of Technology and Metallurgy, University of Belgrade, Karnegijeva 4, 11120 Belgrade, Serbia

[b] Faculty of Technology and Metallurgy, University of Belgrade, Karnegijeva 4, 11120 Belgrade, Serbia

[c] Institute for Multidisciplinary Research, University of Belgrade, Kneza Višeslava 1, 11030 Belgrade, Serbia

[d] National Center for Electron Microscopy, Molecular Foundry, Lawrence Berkeley National Laboratory, Berkeley, 94720 California, United States

[e] Serbian Academy of Sciences and Arts, Knez Mihailova 35, 11000 Belgrade, Serbia

*** Corresponding author**

E-mail: puskokovic@tmf.bg.ac.rs (Petar S. Uskoković)

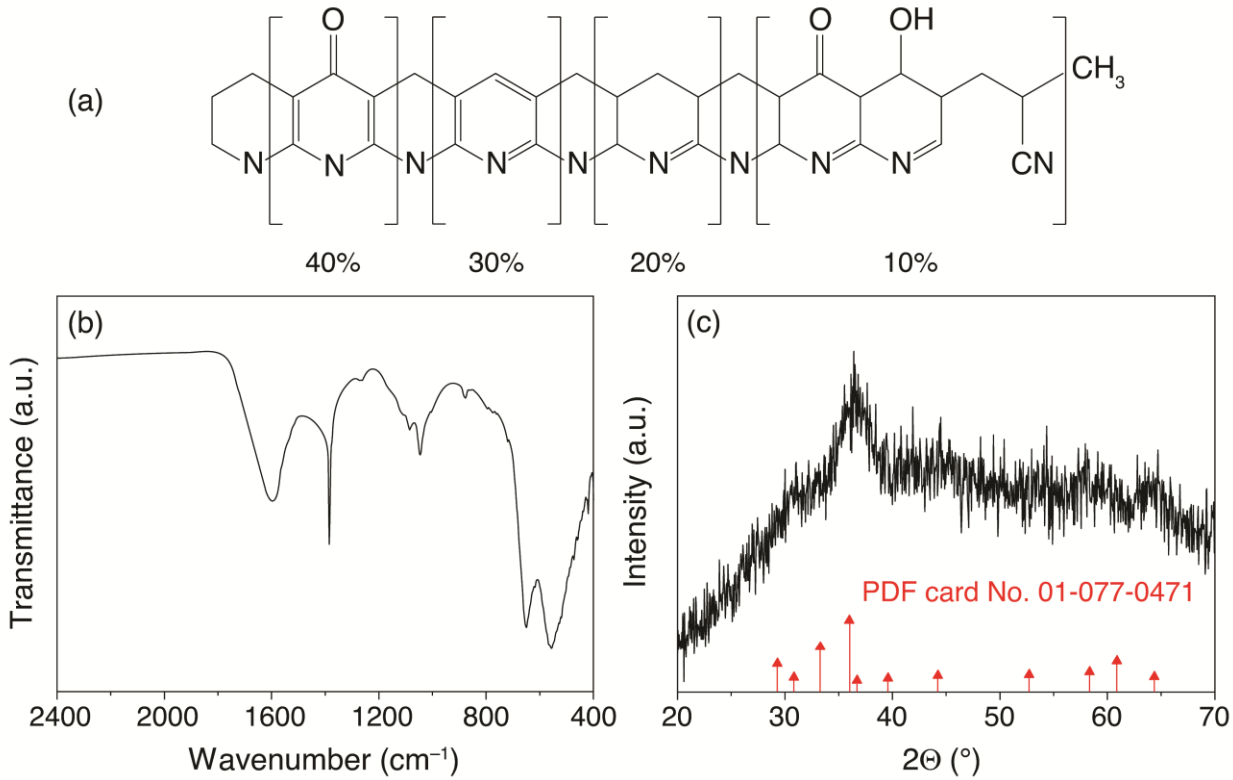

Fig. S1 (a) Proposed stabilized PAN structure[S1]; (b) ATR–FTIR spectrum; and (c) XRD pattern of air–stabilized hybrid fibers with reference PDF card.

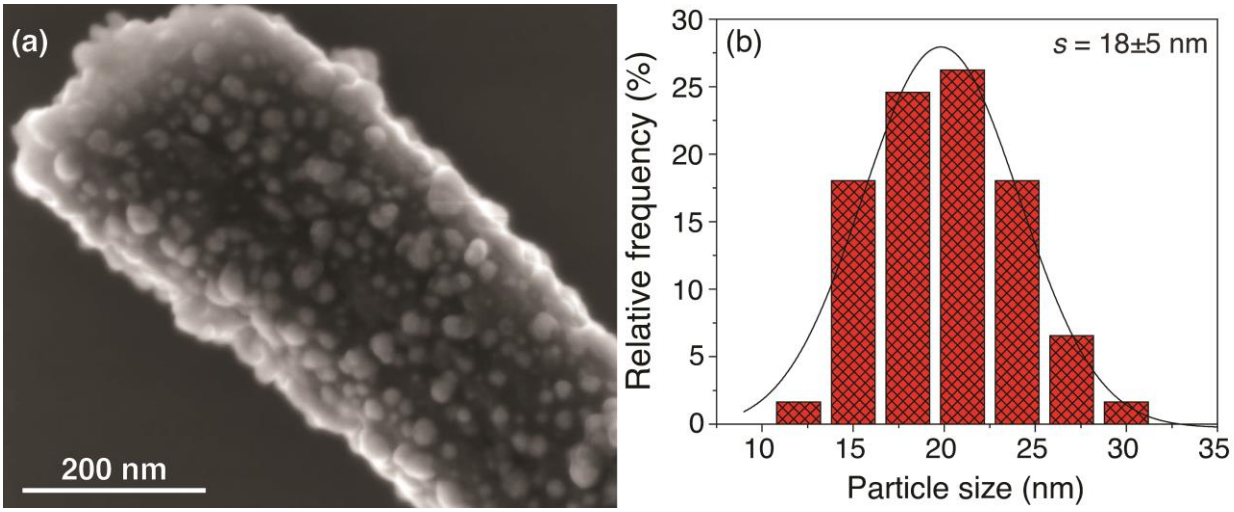

Fig. S2 (a) FE–SEM image of single composite fiber; (b) nanocrystal size distribution.

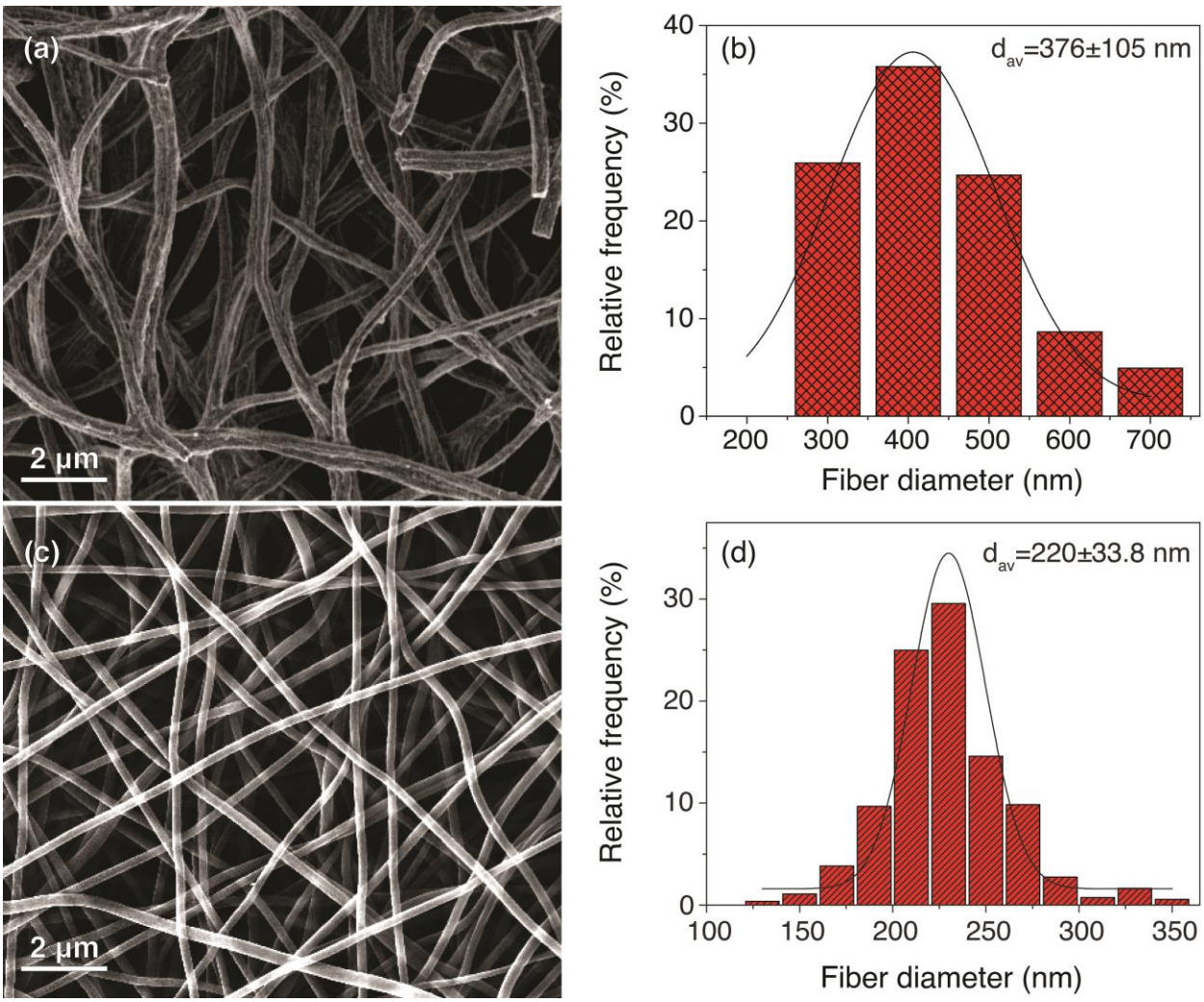

Fig. S3 (a) FE–SEM image of composite fibers with diameter distribution shown in (b); (c) FE–SEM image of bare carbon fibers with diameter distribution shown in (d).

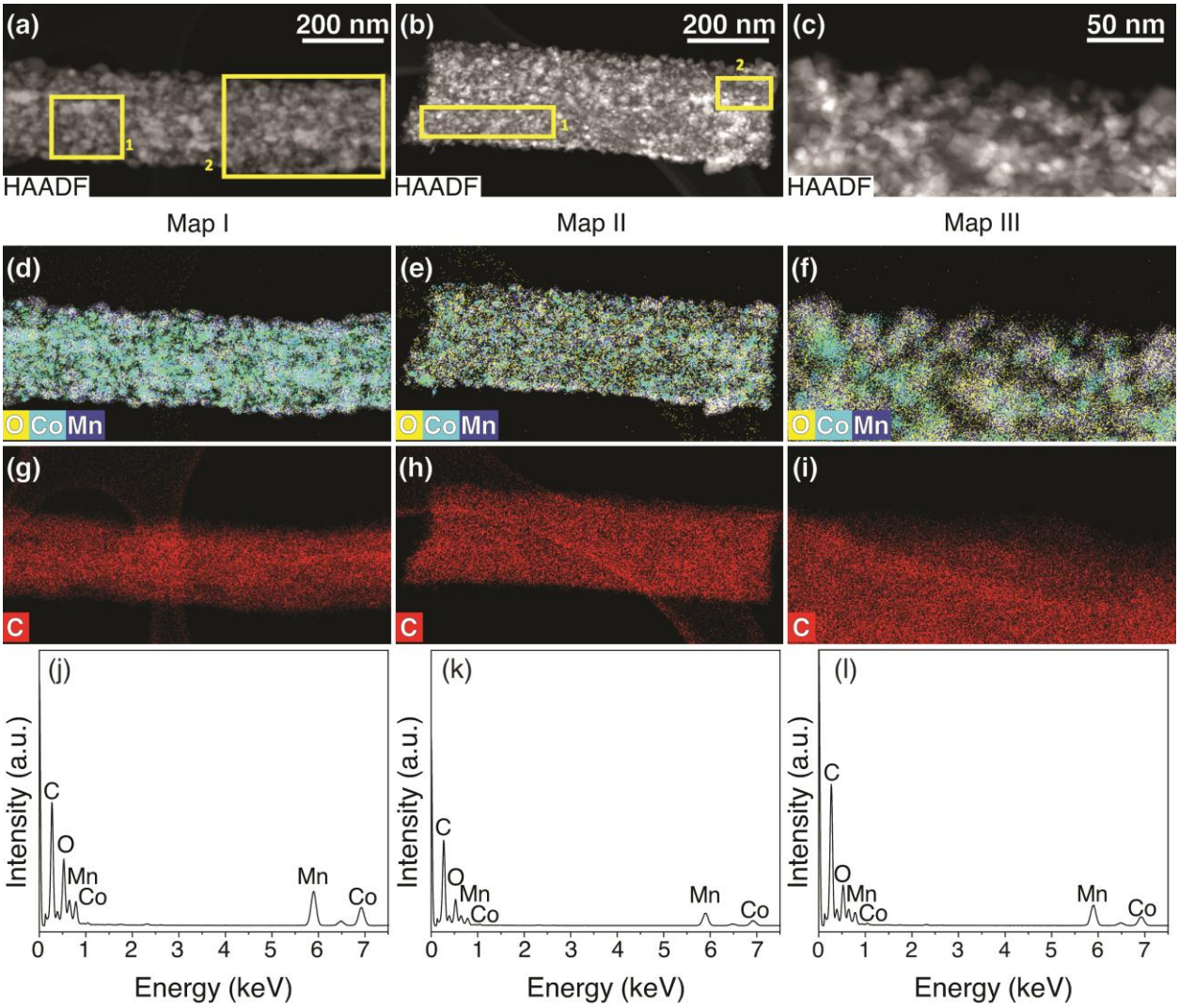

Fig. S4 (a–c) HAADF STEM micrographs of composite fibers with appropriate (d–f) EDS maps of combined – oxygen (O), cobalt (Co) manganese (Mn), as well as (g–i) carbon (C) elemental distribution; (j–l) EDS spectra with noted elements present.

Table S1. Quantification of EDS data from Map I (regions 1 and 2 are noted as rectangles in HAADF micrograph).

Region 1	wt.%	STD	at.%	STD
O	13.8	1.4	16.0	1.6
Mn	23.0	2.3	7.8	0.8
Co	17.2	1.8	5.4	0.6
Region 2	wt.%	STD	at.%	STD
O	14.1	1.4	16.6	1.6
Mn	24.3	2.4	8.3	0.8
Co	16.7	1.7	5.3	0.5

Table S2. Quantification of EDS data from Map II (regions 1 and 2 are noted as rectangles in HAADF micrograph).

Region 1	wt.%	STD	at.%	STD
O	10.2	1.2	9.8	1.2
Mn	16.9	1.9	4.7	0.5
Co	7.7	1.1	2.0	0.3
Region 2	wt.%	STD	at.%	STD
O	9.4	1.4	9.0	1.3
Mn	17.4	2.3	4.9	0.6
Co	7.8	1.4	2.0	0.4

Table S3. Quantification of EDS data from Map III.

	wt.%	STD	at.%	STD
O	10.2	1.0	10.1	1.0
Mn	18.6	1.8	5.4	0.5
Co	9.7	1.0	2.6	0.3

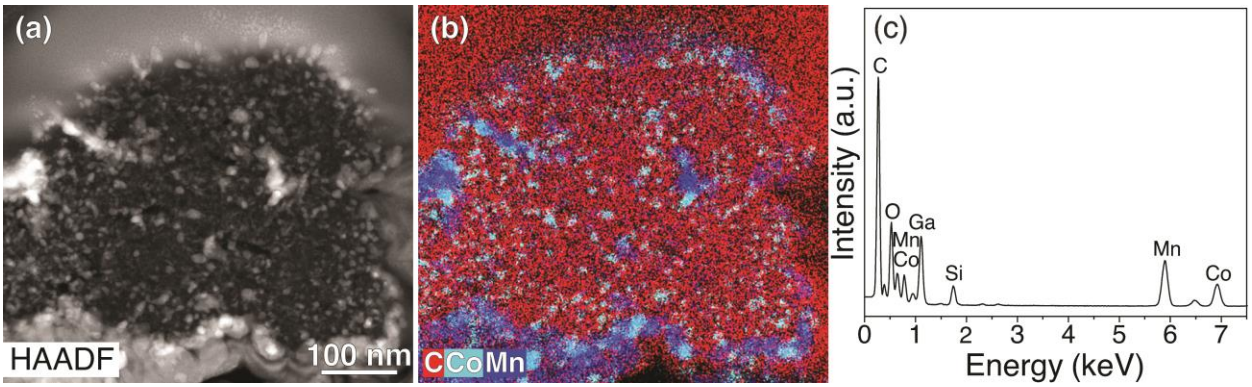

Fig. S5 (a) STEM HAADF micrograph of C@$CoMn_2O_4$ cross–section; (b) appropriate EDS composite map of C (red), Co (turquoise) and Mn (blue) elemental distribution; (c) EDS spectrum with noted elements present in the cross–section.

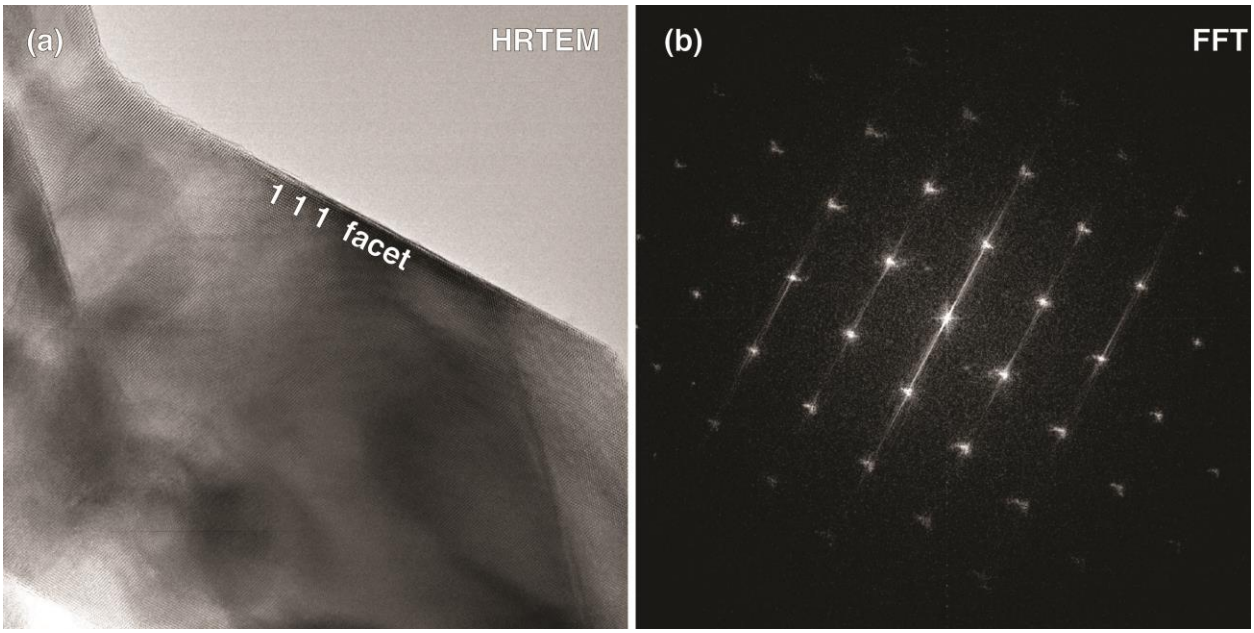

Fig. S6 HRTEM of MnO nanocrystal with noted 111 facet; b) FFT of nanocrystal.

Table S4. EDS quantification from particle above noting that the at.% ratio Mn:O is around 1:1 indicating MnO.

	wt.%	STD	at.%	STD
O	23.0	2.9	50.9	6.4
Mn	66.8	7.3	43.0	4.7
Co	10.1	1.9	6.1	1.1

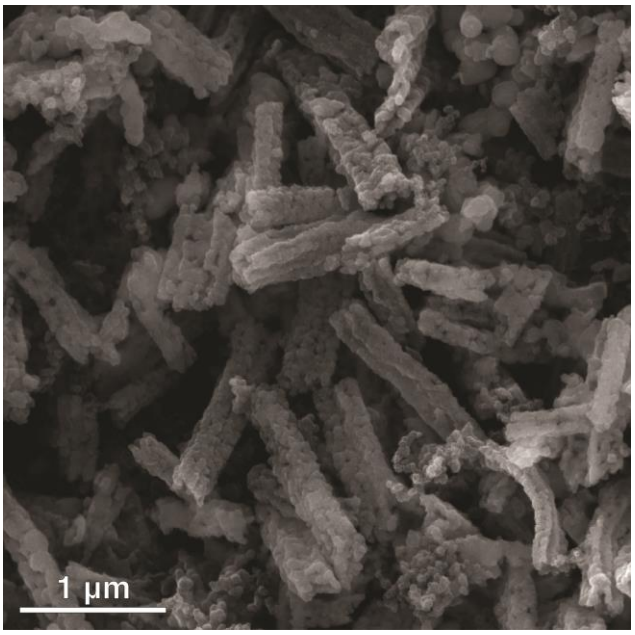

Fig. S7 SEM micrograph of composite electrode after cycling test. Fiber–like morphology with individual nanocrystals can be noted.

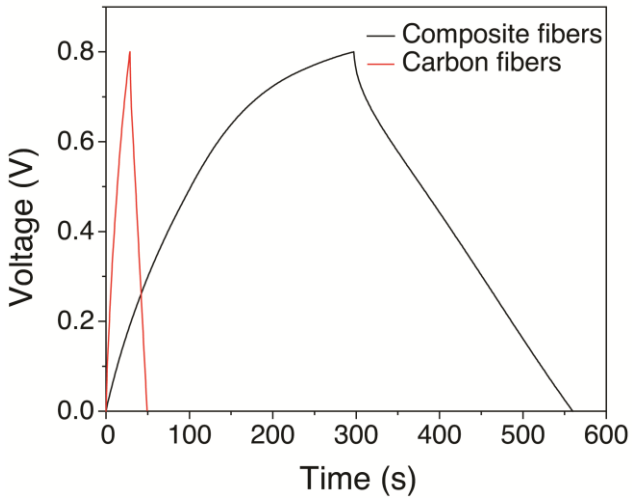

Fig. S8 GCD curves at the current density of 0.5 A g^{-1} for composite (black line) and bare carbon fibers (red line) in the coin–cell device.

The electrochemical performance of bare carbon fibers was evaluated in a coin–cell device over a voltage range of 0 to 0.8 V in 1M KOH aqueous solution. Typical capacitive behavior is indicated by triangular shape of the GCD curve (red line). The specific capacitance and energy density of the individual carbon electrode are around 25.7 F g^{-1} and 0.57 Wh kg^{-1}, respectively, which is around 13 times lower than corresponding values for composite fibers (black line).

Differentiation method by Dunn

The analysis was performed for CV curves at lower sweep rates (5, 10 and 20 mV s^{-1}), shown in Fig. S10, by following the next steps:

1. The potential (V *vs.* SCE) was fixed at a specific value and the current (in mA) was determined for low sweep rates. The example is given for 0.4 V *vs.* SCE (red dashed line and red dots noting current values in Fig. S10).

2. After plotting $i/v^{1/2}$ vs. $v^{1/2}$ (Fig. S11), the slope (k_1) and the intercept (k_2), were determined according to the equation:

$$\frac{i(V)}{v^{1/2}} = k_1 v^{1/2} + k_2$$

3. The current was differentiated at a specific sweep rate as:

$$i_{capacitive} = k_1 v$$

$$i_{diffusion} = k_2 v^{1/2}$$

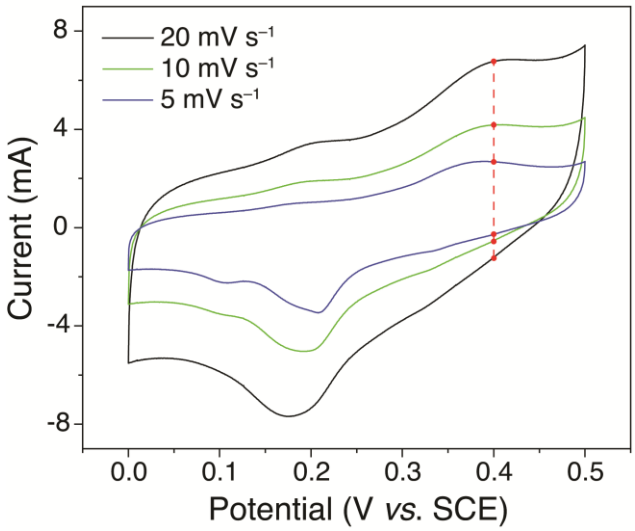

Fig. S9 CV curves of C@$CoMn_2O_4$ composite electrode at low sweep rates (noted in the figure).

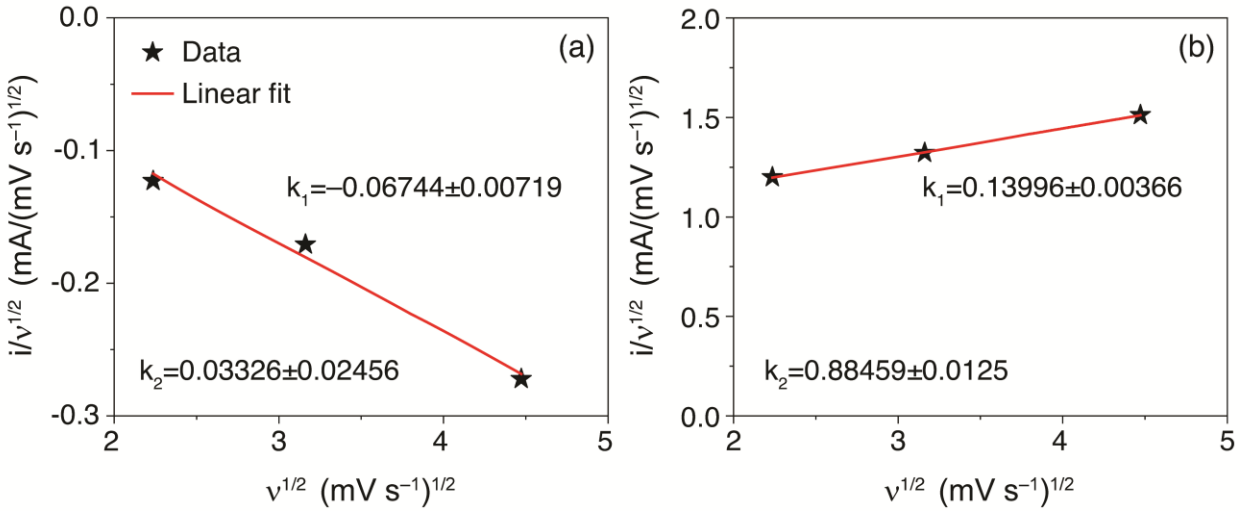

Fig. S10 Linear fit of $i/v^{1/2}$ vs. $v^{1/2}$ values.

4. The steps 1–3 were repeated in a potential range of 0–0.5 V *vs.* SCE with the step of 2 mV. After obtaining the values, we plot charge separation curves as $i_{capacitive}$ *vs.* potential at 5 mV s^{-1} (Fig. 6c noted as the hashed area).

Table S5. Electrochemical performance of composite fibers in 1M KOH solution in conventional three–electrode (3E) cell configuration.

Discharge current density (A g^{-1})	Discharge time (s)	Specific capacity (mAh g^{-1})
1	≈ 225	62.5
2	≈ 106	58.9
3	≈ 66	55.0
5	≈ 35	48.6
10	≈ 13	36.1

Table S6. Performance of transition metal oxides in alkaline electrolytes in the 3E configuration.

Electrode material	Method of fabrication	Electrolyte	Specific capacity *	Cycling stability	Ref.
$C@CoMn_2O_4$	**Electrospinning + calcination**	**1 M KOH**	**~ 62.5 mAh g^{-1} (1 A g^{-1})**	**90 % (4 000 cycles at 10 A g^{-1})**	**Our work**
$CoMn_2O_4$	Co–precipitation method	2 M KOH	~ 34.5 mAh g^{-1} (1 A g^{-1})	No data	[S2]
$CoMn_2O_4@MoS_2$ (10%)			~ 57.1 mAh g^{-1} (1 A g^{-1})	No data	
$CoMn_2O_4@MoS_2$ (20%)			~ 67.5 mAh g^{-1} (1 A g^{-1})	80 % (1 500 cycles at 2 A g^{-1})	
Co_2MnO_4	Hydrothermal method + calcination	1 M KOH	~ 50.0 mAh g^{-1} (1 A g^{-1})	94 % (4000 cycles at 2 A g^{-1})	[S3]
$CoFe_2O_4$	Co–precipitation method	6 M KOH	~ 33.8 mAh g^{-1} (1 A g^{-1})	No data	[S4]
$Co_2MnO_{4.5}$	Hydrothermal method + calcination	1 M KOH	~ 16.5 mAh g^{-1} (1 A g^{-1})	100 % (2 000 cycles at at current densities from 1 to 10 A g^{-1})	[S5]
$CuCo_2O_4$	Solution combustion method	3 M KOH	~ 44.0 mAh g^{-1} (1 A g^{-1})	86 % (1 000 cycles at 10 A g^{-1})	[S6]
Co_2MnO_4	Solvothermal method	1 M KOH	~ 44.8 mAh g^{-1} (2 A g^{-1})	No data	[S7]
Co_2MnO_4@VCFs			~ 48.4 mAh g^{-1} (2 A g^{-1})	107 % (10000 cycles at 5 A g^{-1})	
CNF@NiO	Electrospinning + calcination	6 M KOH	~ 58.3 mAh g^{-1} (1 A g^{-1})	No data	[S8]
$CoFe_2O_4$/FeOOH	Hydrothermal method	6 M KOH	~ 44.2 mAh g^{-1} (1 A g^{-1})	91.3 % (1000 cycles at 5 A g^{-1})	[S9]
$ZnFe_2O_4$@NRG	Solvothermal method + calcination	1 M KOH	~ 54.5 mAh g^{-1} (1 A g^{-1})	83.8 % (5000 cycles at 100 mV s^{-1})	[S10]

aCF@$ZnFe_2O_4$	Solution processing + annealing	2 M KOH	~ 59 mAh g^{-1} (1 A g^{-1})	92.7 % (20 000 cycles at 2 A g^{-1})	[S11]
$ZnCo_2O_4$@CNF	Electrospinning + thermal treatment	6M KOH	~ 29.6 mAh g^{-1} (1 A g^{-1})	125 % (1 000 cycles at 1 A g^{-1})	[S12]
Co_3O_4@CNF	Electrospinning + thermal treatment	6 M KOH	~ 43/48/81 mAh g^{-1} (1 A g^{-1})	74 % (2 000 cycles at 2 A g^{-1})	[S13]
Fe_3O_4@MWCNT	Hydrothermal method	6 M KOH	~ 39 mAh g^{-1} (1 A g^{-1})	100% (2 000 cycles at 10 mA cm^{-2})	[S14]

***** Specific capacity values (mAh g^{-1}) were re-calculated according to equation (3).

Table S7. The capacitive parameters of the individual C@$CoMn_2O_4$ electrode in the coin–cell device calculated from CV and GCD measurements based on active mass of the electrode.

Sweep rate ($V\ s^{-1}$)	$C_{s,coin,CV}$ ($F\ g^{-1}$)	$E_{d,CV}$ ($Wh\ kg^{-1}$)	$P_{d,CV}$ ($kW\ kg^{-1}$)
0.005	277	≈ 6.2	≈ 0.138
0.010	246	≈ 5.5	≈ 0.246
0.050	172	≈ 3.8	≈ 0.858
0.100	137	≈ 3.1	≈ 1.372
Discharge current density* ($A\ g^{-1}$)	$C_{s,coin,GCD}$ ($F\ g^{-1}$)	$E_{d,GCD}$ ($Wh\ kg^{-1}$)	$P_{d,GCD}$ ($kW\ kg^{-1}$)
0.5	329	≈ 7.3	≈ 0.1
1	305	≈ 6.8	≈ 0.2
3	270	≈ 6.0	≈ 0.6
6	202	≈ 4.5	≈ 1.2
12	135	≈ 3.0	≈ 2.4

* based on active mass of the individual electrode

Literature

[S1] B. Saha and G.C. Schatz, *J. Phys. Chem. B*, 2012, **116**, 4684−4692.

[S2] N. Kanaujiya, N. Kumar, M. Singh, Y. Sharma and G.D. Varma, *J. Energy Storage*, 2021, **35**, 102302.

[S3] L. Li, Y.Q. Zhang, X.Y. Liu, S.J. Shi, X.Y. Zhao, H. Zhang, X. Ge, G.F. Cai, C.D. Gu, X.L. Wang and J.P. Tu, *Electrochim. Acta*, 2014, **116**, 467–474.

[S4] H. Kennaz, A. Harat, O. Guellati, D.Y. Momodu, F. Barzegar, J.K. Dangbegnon, N. Manyala and M. Guerioune, *J. Solid State Electrochem.*, 2018, **22**, 835–847.

[S5] W. Li, K. Xu, G. Song, X. Zhou, R. Zou, J. Yang, Z. Chen and J. Hu, *CrystEngComm*, 2014, **16**, 2335–2339.

[S6] A. Pendashteh, M.S. Rahmanifar, R.B. Kaner and M.F. Mousavi, *Chem. Commun.*, 2014, **50**, 1972–1975.

[S7] M. Nagaraju, S.C. Sekhar, S.J. Arbaz and J.S. Yu, *Appl. Surf. Sci.*, 2021, **563**, 150223.

[S8] Q. Li, J. Guo, D. Xu, J. Guo, X. Ou, Y. Hu, H. Qi and Feng Yan, *Small*, 2018, **14**, 1704203.

[S9] Y.X. Zhang, X.D. Hao, Z.P. Diao, J. Li and Y.M. Guan, *Mater. Lett.*, 2014, **123**, 229–234.

[S10] L. Li, H. Bi, S. Gai, F. He, P. Gao, Y. Dai, X. Zhang, D. Yang, M. Zhang and P. Yang, *Sci. Rep.*, 2017, **7**, 43116.

[S11] S. Yang, Z. Han, F. Zheng, J. Sun, Z. Qiao, X. Yang, L. Li, C. Li, X. Song and B. Cao, *Carbon*, 2018, **134**, 15–21.

[S12] H. Yu, H. Zhao, Y. Wu, B. Chen and J. Sun, *J. Phys. Chem. Solids*, 2020, **140**, 109385.

[S13] S. Abouali, M.A. Garakani, B. Zhang, Z.-L. Xu, E. K. Heidari, J.-Q. Huang, J. Huang and J.-K. Kim, *ACS Appl. Mater. Interfaces*, 2015, **7**, 13503–13511.

[S14] D. Guan, Z. Gao, W. Yang, J. Wang, Y. Yuan, B. Wang, M. Zhang and L. Liu, *Mater. Sci. Eng. B*, 2013, **178**, 736–743.